Oral Science International, November 2008, p.85–95

Development of Computer-assisted Diagnosis Using Digital Radiography for the Evaluation of Dental Implant Osseointegration

Kiyonobu Hayashi, Yusuke Kaku, Ryota Kawamata, Koji Nakamura, Takashi Sakurai and Isamu Kashima

Division of Radiology, Department of Maxillofacial Diagnostic Science, Kanagawa Dental College

Abstract: To develop an osseointegration analyzing system for dental implants, a new analyzing system which can assess the level of osseointegration between an implant and trabecular bone was constructed using digital radiography with morphological filter and node-strut analysis. For assessment of this system, a grayscale test chart that simulates six levels of an osseointegration was created. In addition, digital implant images were made in which the trabecular pattern around the implant was varied over a total of five levels. Implant osseointegration was evaluated on the basis of seven parameters related to the number of nodes (Nd) and terminuses (Tm) of the skeleton bound to the implant (Im) and the skeletal length. The seven parameters were as follows: the number of struts connecting the Im with the Nd and Tm (N.ImNd, N.ImTm), the total number of N.ImNd and N.ImTm (N.Im), the strut length connecting the Im with the Nd and Tm (ImNd, ImTm), and the ratios of the struts connecting the Im with the Nd and Tm (ImNd/TSL, ImTm/TSL), where TSL is the total strut length.

Strong correlations (R^2 = 0.971–1.0) between the theoretical values from the test charts and the measured values were demonstrated. N.ImNd showed the strongest correlation, R^2 = 0.948, from the digital implant images, followed by N.Im and ImNd, with correlations of R^2 = 0.86 and R^2 = 0.84, respectively. This new system for evaluating implant osseointegration by applying morphological processing and node-strut analysis could be useful for computer-assisted diagnosis of digital dental implant images.

Key words: dental implant, digital radiography, osseointegration, computer-assisted diagnosis

Introduction

Conventional methods of objectively evaluating implant stability include removal tests and removal torque measurements, but these methods are destructive and not suitable for clinical applications[1–3]. Cutting resistance measurements at the time of implantation are non-destructive and permit objective evaluation of implant stability, but do not enable longitudinal assessment of the changes after the implantation[4,5]. Tooth mobility measurements and resonance frequency analysis (RFA) enable objective and longitudinal assessment of the changes. Tooth mobility measurements are expressed as periotest values[6–8]. However, for implants for which sufficient osseointegration has not been achieved, there may

Received 3/25/08; revised 8/12/08; accepted 8/22/08.
Requests for reprints: Takashi Sakurai, Division of Radiology, Department of Maxillofacial Diagnostic Science, Kanagawa Dental College, 82 Inaoka, Yokosuka, Kanagawa, 238-8580, Japan, Phone: 046-822-8851, Fax: 046-822-8851, E-mail: sakurait@kdcnet.ac.jp

be a loss of osseointegration due to the loading at the time of measurement. In consideration of these various problems, a nondestructive method using RFA was recently developed for evaluating implant stability, and the results of its clinical application have been reported[9–16]. With the RFA method, a transducer is immobilized above the implant, and the characteristic vibration frequency of the implant is measured[17–18]. This method is widely used in industry to identify flaws, cracks and damage in structures that are comprised of uniform metals or cement[19]. However, bones are comprised of dense cortical bone and cancellous bone that has a three-dimensional mesh-like structure. In addition, the proportions of these bone components may vary largely due to individual differences and the area of the bone. Therefore, the ability of RFA to reflect the status between the jaw bone and an implant is unknown.

On the other hand, European and American guidelines for implant therapies recommend that X-ray tomography of one tooth or a small area, or computed tomography (CT) of an area including multiple teeth, be carried out together with conventional radiography (intraoral radiography, occlusal radiography, panoramic radiography and lateral cephalometric radiography) as imaging diagnosis prior to implantation surgery[20,21]. In particular, CT has been used for preoperative evaluation of bone quality[22–27], and in recent years there have also been reports of preoperative imaging diagnosis using magnetic resonance imaging (MRI)[28–32]. However, applications of CT and MRI for postoperative imaging diagnosis aimed at monitoring the course following implantation still have problems such as artifacts and resolution. Moreover, for judging the prognosis after implantation, it is important to evaluate the relationship between the implant and the surrounding trabecular bone structure. It was also reported that secondary implant stability was increased due to bone formation and remodeling at the implant/tissue interface and in the surrounding bone[8]. For that reason, presently the postoperative prognosis of implants is visually evaluated by using intraoral radiography. In consideration of this background, the authors have been developing a technologically simple and economical method for longitudinal evaluation of the osseointegration of implants.

The objective of this study was to develop a computer-assisted diagnosis based on digital radiography for longitudinal, quantitative evaluation of the relationship between implants and the surrounding trabecular bone structure.

Materials and Methods

1. Implant osseointegration analyzing system

Figure 1 shows a block diagram of the system used in this study for analyzing implant osseointegration. Two kinds of original digital implant images were prepared for evaluating the accuracy of the system. The digital implant images of one group were constructed by commercial graphic software (Adobe Illustrator CS ver. 11.0, Adobe System Inc., CA, USA) as grayscale test chart images. The digital implant images of another group were obtained from a test phantom of an implant on a bone block using a digital X-ray imaging system (FCR 5000 MA Plus, Fuji Photo Film, Tokyo, Japan). The region of interest (ROI) for analysis was established in the original digital implant image. Noise was removed from the digital radiographic imaging data of the trabeculae in the ROI by filter processing (mask size, 3 × 3 pixels). The skeletal features of the trabeculae were extracted from the digital image data using a disk-shaped single structuring element with a diameter of 5 pixels, and images of the skeletal features were produced. The operation number was 3–6, and the skeletal features were extracted in trabeculae of width greater than 650 μm. The equation used for this analysis was a skeletal operation[33–37]. After the skeletal grayscale images were binarized at a threshold level of 1.0, isolated skeletal components of less than 20 pixels were removed by a selective skeletal filtering process. The skeletal area (Sk.Ar) was determined by morphometric indices calculated from the binary image data. Sk.Ar is a relative assessment of the quantity of skeletal structure in the entire tissue area.

Skeletal features of a width of 1 pixel were extracted from the binary image data by a thin-

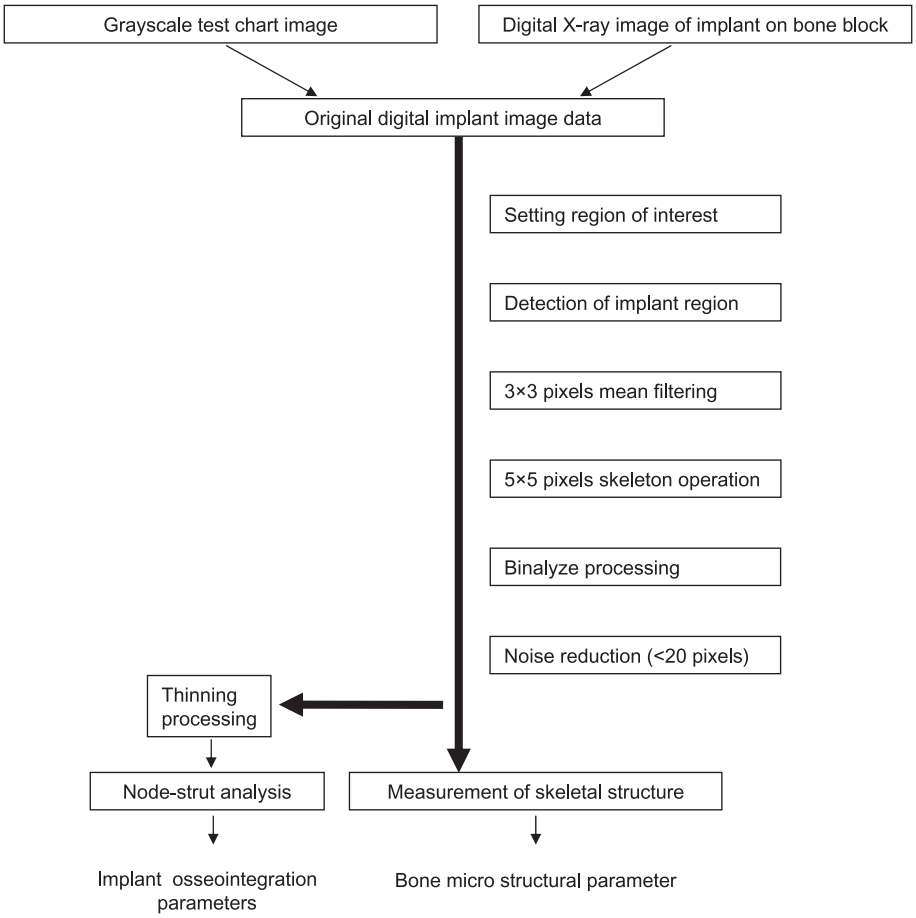

Fig. 1 Flow diagram illustrating the procedure used for the implant osseointegration analyzing system in this study. The system consists of detection processing of the implant body, mask size 3 × 3 pixel mean filtering, morphological filtering based on mathematical morphology (binarized processing, 5 × 5 pixel skeleton operation), and measurement of the skeletal structure and node-strut analysis.

ning process for implant osseointegration analysis. Node-strut analysis was applied to quantify the connectivity of the trabecular skeletal elements and implant body using the 1-pixel-wide skeletal image data. In the present study, a point at which three or more trabecular skeletal elements intersect defines a node (Nd), and a terminating end point, which is a point that is not contiguous with other skeletal elements, defines a terminus (Tm). The struts are defined as linear skeletal elements[38,39]. In the developed analyzing system, the number of struts connecting the implant with the Nd (*i.e.*, N.Im, N.ImNd and N.ImTm), the strut length (*i.e.*, ImNd and ImTm) and the ratios of the strut lengths to the total strut length (TSL) (*i.e.*, ImNd/TSL and ImTm/TSL) were defined as the implant osseointegration parameters. These parameters of node-strut analysis show higher values as the osseointegration between the implant and the surrounding trabecular bone advances. Conversely, if the osseointegration fails and/or the interface between the implant and the bone trabeculae decreases, these parameters show lower values.

2. Grayscale test chart images

To evaluate the precision of the implant osseointegration analyzing system, six images of a rectangular binary test chart were created on a cathode ray tube (CRT) that simulated the Nd, Tm and implant body within 50 pixels in width and 200 pixels in length. The trabeculae were cre-

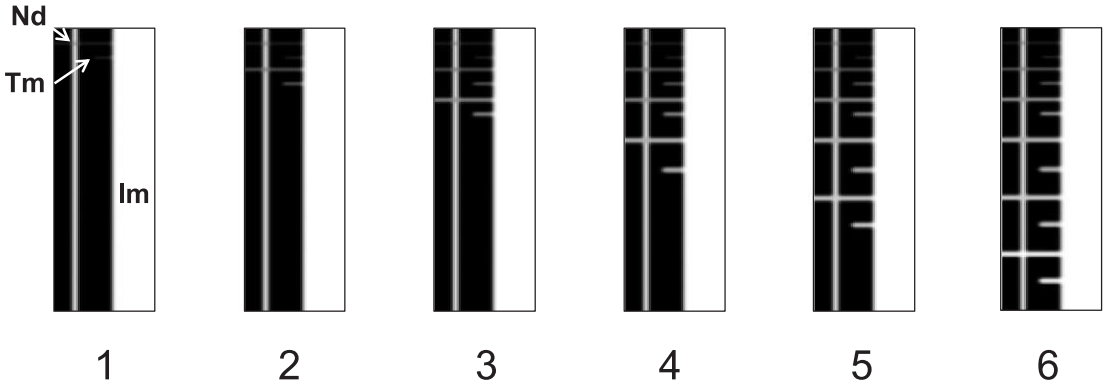

Fig. 2 Image of the grayscale test chart created on the CRT. The number and width of the trabeculae connecting to the implant (Im) were varied over six levels.

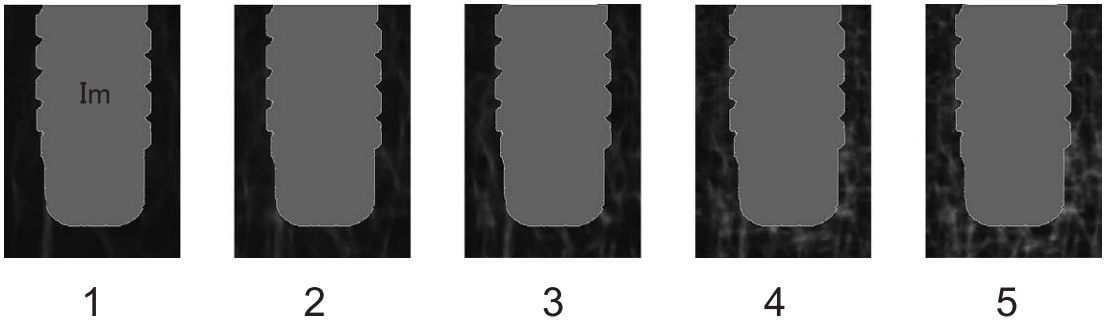

Fig. 3 Digital implant test phantom radiographic images with the trabeculae surrounding the Im varying over five levels.

ated with longitudinal and horizontal lines that intersected at 90° degrees. The width of the horizontal line was varied between 1–6 pixels, and the brightness was changed from 100% to 50% in stages for each line. In addition, by means of Gaussian filter processing with a diameter of 3 pixels, the binary test chart was resynthesized as grayscale test chart images having a characteristic X-ray image penumbra. Figure 2 shows the grayscale test chart images that were created with six levels on the CRT.

3. Digital implant test phantom image data

Excised bone block from a human femoral neck, which has dense bone trabeculae, was cut into five 2-mm sections and 1.5-mm phantoms were prepared by placing a material that was equivalent to the cortical bone on both the X-ray tube side and the imaging plate (IP; Fuji Photo Film) side. The bone trabeculae of the femoral neck consist almost entirely of longitudinal, horizontal and oblique structures, whereas the mandible has more complicated structures. Therefore, the bone trabecular structures of both bones are somewhat different. However, the bone block of the femoral neck was used for the sake of convenience of preparing the bone block slices, because the bone block of the femoral neck has sufficient thickness for making multilayer slices. A screw-type titanium implant (Straumann, Switzerland) was placed on the first thickness step of the cancellous bone block, because it was difficult to drill a hole for implant in the bone block of 2 mm thickness without destroying cancellous bone. Standardized radiography was performed at each of the five thickness steps of the cancellous bone. Radiographs were obtained with a standard-type IP for computed radiography (CR; Fuji Photo Film) and a microfocus X-ray tube (P70-Ⅱ, Pony Anatomic, Tokyo, Japan). The exposure conditions were 30 kV, 90 μA, 20 seconds, focus to an IP distance of 33 cm and to a subject distance of 11 cm at 3 times the magnification imaging. The original images were scanned with a FCR 5000 MA Plus. Figure 3 shows

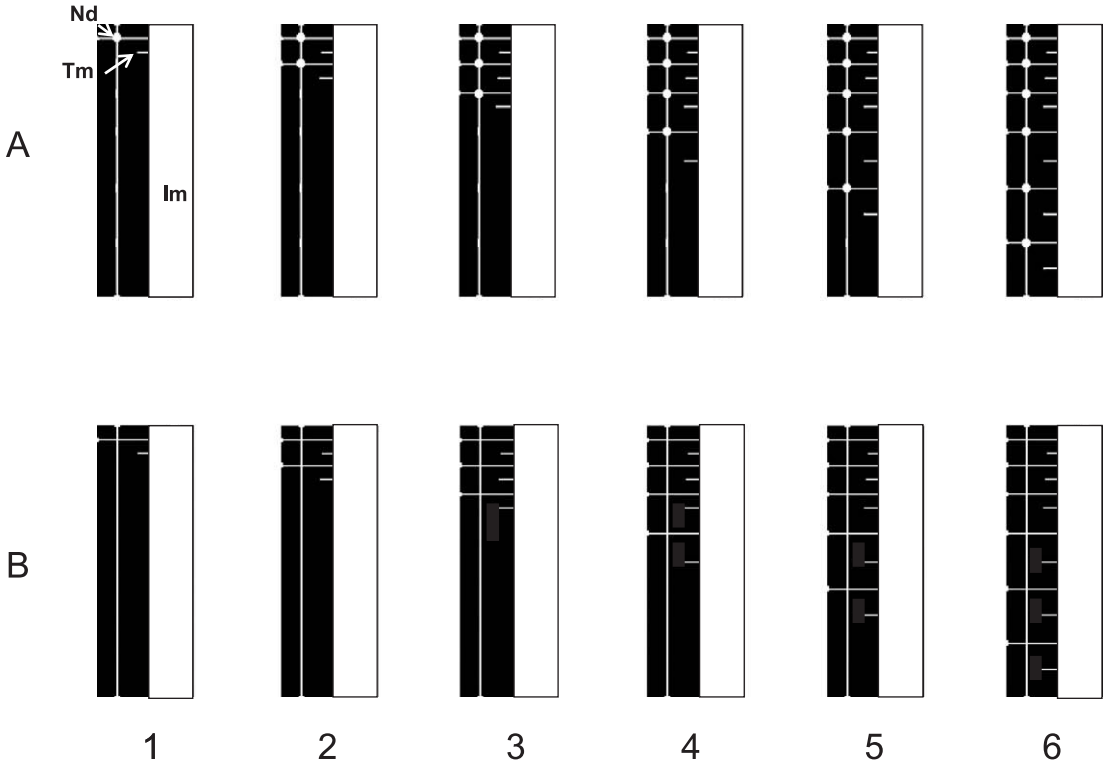

Fig. 4 (A) Skeletal images of the grayscale test chart obtained by morphological processing and (B) thinning processing images. Trabeculae having different density and thickness were extracted as the skeleton of constant thickness. It is possible to visually confirm the 1–6 Nd and Tm binding to the implant (Im) on the six-level test chart images.

the digital implant test phantom images with the trabecular patterns around the implant varied over five levels from coarse to dense, obtained by standardized radiography using bone block and titanium implant.

Results

Figure 4 shows (A) the six step skeletal images of grayscale test chart created by morphological processing and (B) the thinning processing images. For both the skeletal and thinning processing images, it is possible to visually confirm the 1–6 number of Nd and Tm bindings to the implant. The skeletal images were evaluated quantitatively by calculating morphometric indices as the bone micro structural parameter. The thinning processing images were also evaluated by node-strut analysis as the implant osseointegration parameters. The relationships between the theoretical values of the grayscale test chart and the measurement values obtained by the analysis were analyzed by linear regression. The regression coefficients of each parameter are shown in Table 1. The regression coefficients for Sk.Ar and TSL with each of the skeletal test charts were $R^2 = 0.934$ and $R^2 = 0.988$, respectively; these represent nearly linear relationships. These results confirm that the morphology was processed with a high precision to the grayscale test chart created on the CRT. A high degree of correlation ($R^2 = 0.994–1.0$) was found between the theoretical values and the actual measured values for the number of Nd (N.ImNd), Tm (N.ImTm) and the total number of Nd, Tm (N.Im) connecting to the implant. In addition, the regression coefficient was $R^2 = 1.0$ between the theoretical values and the actual measured values for the strut lengths connecting Nd and Tm to the implant (*i.e.*, ImNd and ImTm). These results demonstrate that the node-strut analysis was carried out with a high precision. The proportional strut lengths connecting Nd and Tm to the implant relative to the TSL (*i.e.*, ImNd/TSL and ImTm/TSL) also showed high regression coeffi-

Table 1 Correlation between theoretical values and measurement values of grayscale test chart images.

Parameters	Regression Coefficients (R^2)
Skeletal Area (Sk.Ar)	0.934
Total Strut Length (TSL)	0.988
Total Number of Nd and Tm (N.Im)	1.000
Number of Nd (N.ImNd)	1.000
Number of Tm (N.ImTm)	0.994
Strut Length Connecting Nd to Implant (ImNd)	1.000
Strut Length Connecting Tm to Implant (ImTm)	1.000
Proportional Strut Length Connecting Nd to Implant Relative to TSL (ImNd/TSL)	0.992
Proportional Strut Length Connecting Tm to Implant Relative to TSL (ImTm/TSL)	0.971

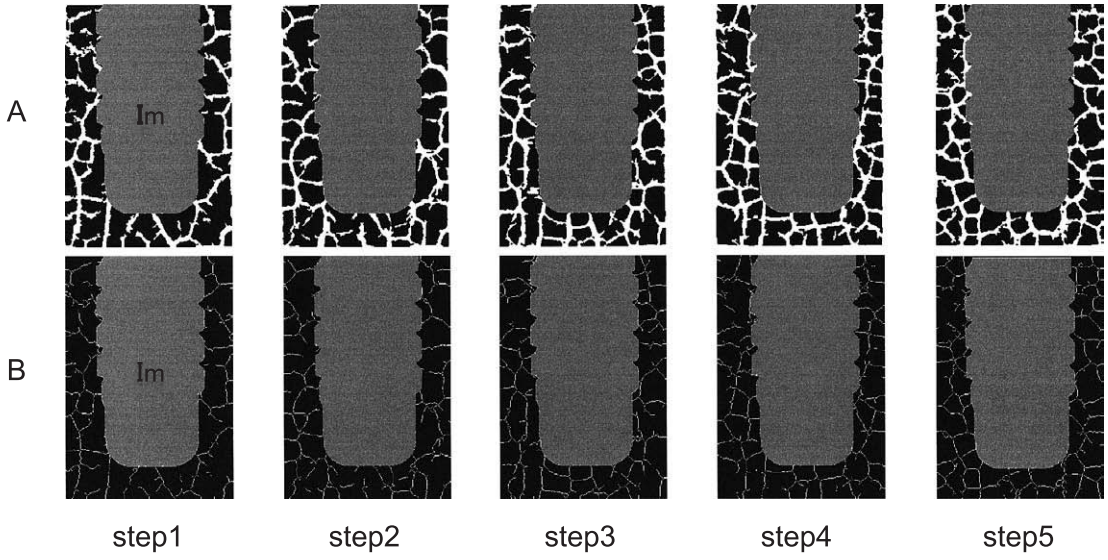

Fig. 5 (A) Skeletal image and (B) thinning processing image obtained by morphological processing of the grayscale digital implant test phantom images of the trabeculae surrounding the implant (Im) with variations over five levels. It was possible to visually confirm that the trabeculae, binding to the implant with variations over five levels from coarse to dense, were extracted as skeletal variations.

cients. The correlation coefficients (R^2 = 0.992 and R^2 = 0971, respectively) revealed nearly proportional relationships between the actual measured values and the theoretical values for these parameters, confirming that the theoretical values are reflected nearly as much as the actual measured values relative to the grayscale test charts having no noise component.

Figure 5 presents (A) the skeletal image and (B) the thinning processing image obtained by morphological processing of the grayscale digital implant test phantom images with the pattern of the trabeculae surrounding the implant varying over five levels. With both the skeletal image and the thinning processing image, it was possible to visually confirm that the skeletal structure binding to the implant showed variations over the five levels from coarse to dense. Figure 6 depicts the relationship between the five levels of digital implant test phantom images and the Sk.Ar/T.Ar and TSL/T.Ar. Strong correlations of R^2 = 0.982 and R^2 = 0.843 were found between the skeletal variations and Sk.Ar and TSL, respectively. These results indicate that each of the digital implant test phantom images simulated the different levels of variation in the trabeculae surrounding the implant with a high degree of accuracy. It was also clarified that, by morphological processing, the variations in the trabeculae were extracted in the skeleton with a high precision.

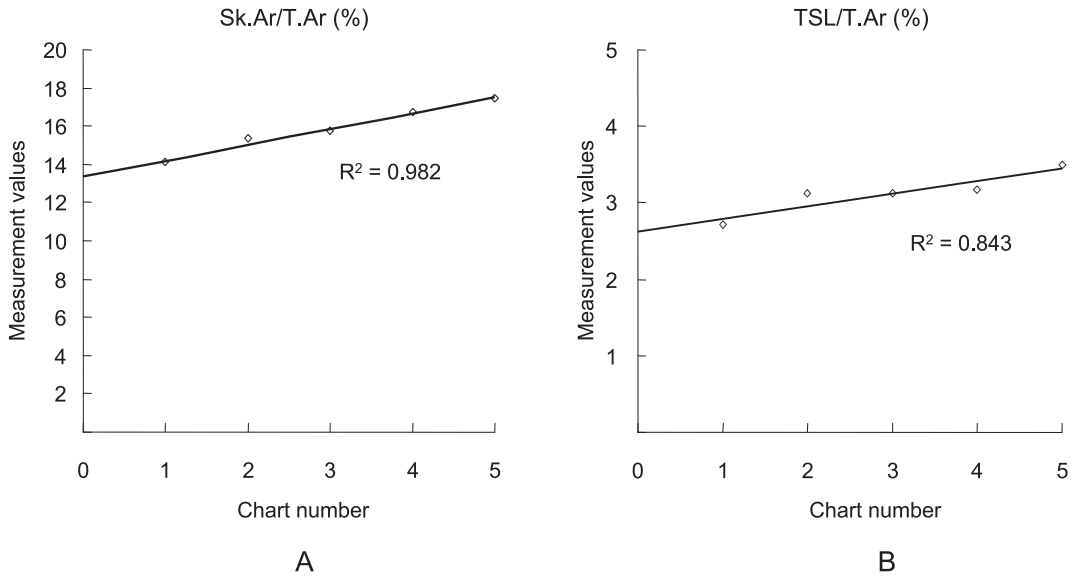

Fig. 6 Relationships between the five-level grayscale digital implant test phantom images and the Sk.Ar and TSL measured using the implant osseointegration analyzing system.

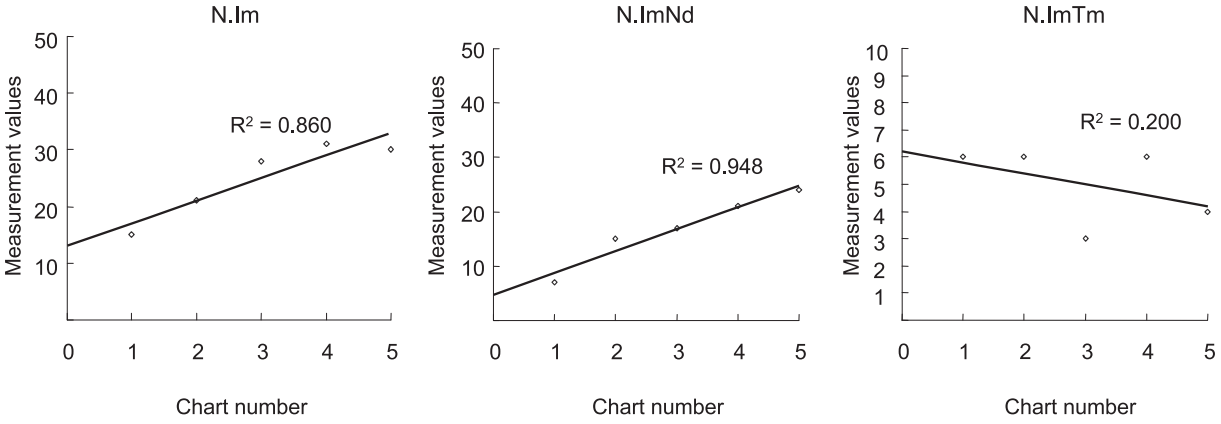

Fig. 7 Relationships between the five-level grayscale digital implant test phantom images and the number of struts connecting each Nd and Tm to the implant (Im) (*i.e.*, N.ImNd and N.ImTm) and the number of connecting points between the Im and the skeleton (N.Im) measured using the implant osseointegration analyzing system.

Figures 7 through 9 present the results of the node-strut analysis of the digital implant test phantom image data that were subjected to the thinning processing shown in Fig. 5 (B). The horizontal axis shows the images of the skeletal variations simulated into five levels, and the vertical axis shows each of the measured values. As shown in Fig. 7, a strong correlation of $R^2 = 0.948$ was demonstrated for N.ImNd among the parameters relating to the number of Nd and Tm binding to the implant. However, no correlation was found for N.ImTm, since the coefficient was $R^2 = 0.2$. A strong correlation of $R^2 = 0.860$ was found for N.Im, a parameter expressing the total number of Nd and Tm binding to the implant. In addition, as shown in Fig. 8, with regard to the parameters relating to the lengths of the struts connecting Nd and Tm to the implant, a strong correlation with $R^2 = 0.84$ was found for ImNd, but no correlation was found for ImTm. As shown in Fig. 9, no correlations were found between the skeletal variations and the parameters relating to the proportional strut lengths connecting each Nd and Tm to the implant, *i.e.*, ImNd/TSL and ImTm/TSL.

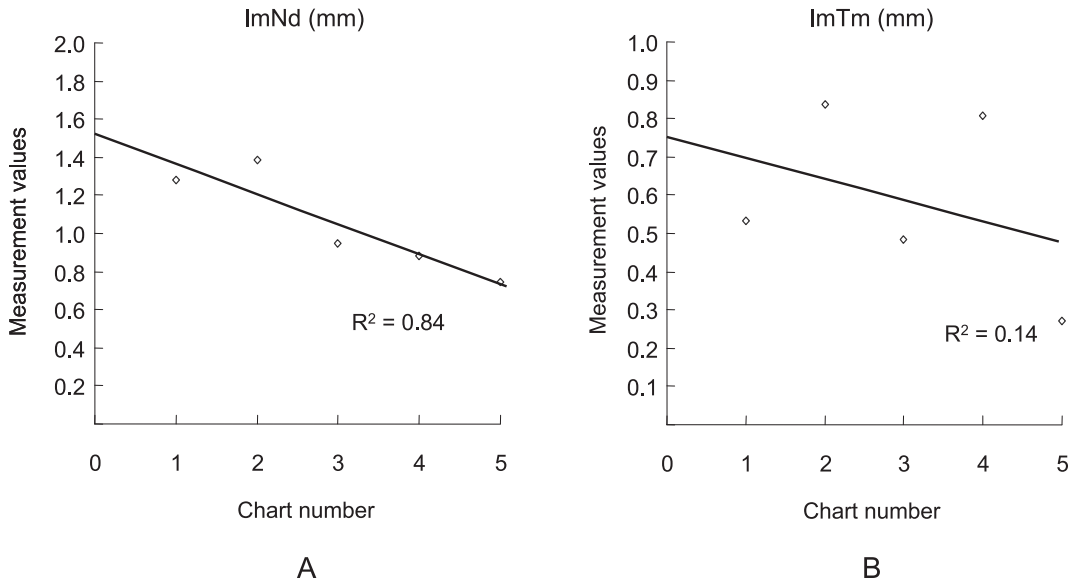

Fig. 8 Relationships between the five-level grayscale digital implant test phantom images and the strut lengths connecting each Nd and Tm to the implant (Im) (*i.e.*, ImNd and ImTm) measured using the implant osseointegration analyzing system.

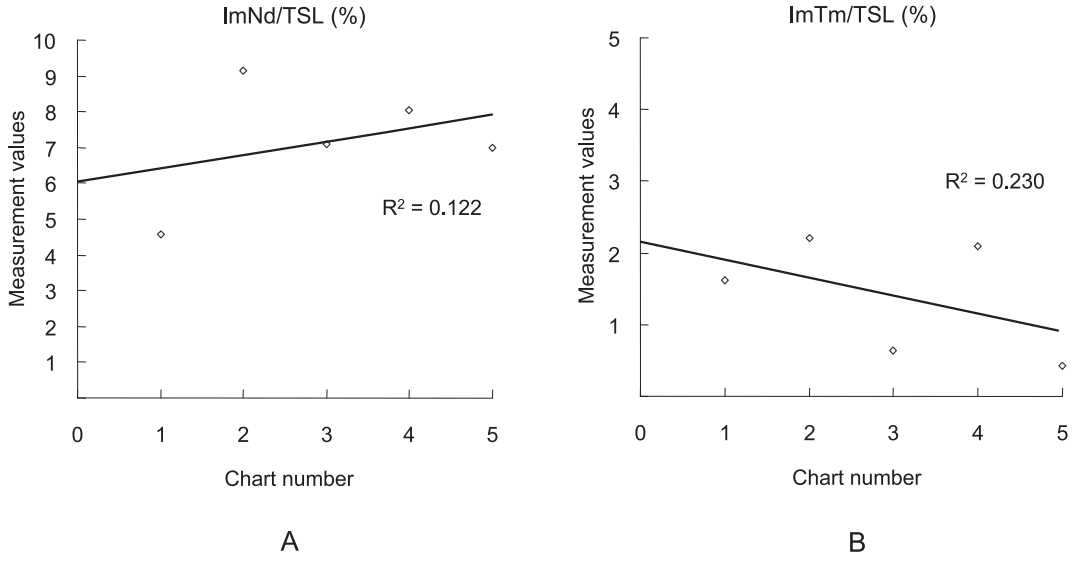

Fig. 9 Relationships between the five-level grayscale digital implant test phantom images and the proportional strut lengths connecting each Nd and Tm to the implant (Im) relative to the total strut length (TSL) (*i.e.*, ImNd/TSL and ImTm/TSL), as determined using the implant osseointegration analyzing system.

Discussion

We took advantage of the characteristics of digital radiography and constructed a new system for evaluating the osseointegration of implants by digitalizing the implant interface between implant body and trabecular bone. This new system is based on morphological processing of the trabecular bone surrounding the implant and extraction of the skeletal structure (Fig. 1). Conventionally, skeletal structures obtained by morphological processing have been quantified as morphometric calculation indices using bone morphometric analysis[34–38]. However, the secondary implant stability depends on the strength of osseointegration

between the implant and the surrounding bone tissue[8]. For that reason, our new system incorporates an improved version of the node-strut method, which evaluates the skeletal structure that is integrated into the implant based on the assumption that it has a structure consisting only of points and lines. Accordingly, the characteristic feature of this new system is that it defines the skeletal structure that is integrated with the implant as the combination of two components, Nd and Tm, and achieves quantification of the skeletal structure.

We then applied our new implant osseointegration analyzing system to a clear test chart of the numbers of Nd and Tm that was created on a CRT (Fig. 2). The noise component, magnification rate, geometric distortion and displacement were eliminated. The results showed that there was a nearly proportional relationship between the theoretical values and actual measured values for parameters relating to both Nd and Tm (Table 1). This means that our new system allows the two-dimensional test charts to be nearly perfectly quantified. These results confirm that the system can accurately extract and quantify the skeletal structure that has integrated with the implant body. Moreover, the results show that the new system is able to carry out a series of image processing steps with a high degree of precision such as detection of the Nd and Tm by node-strut analysis, detection of the implant body, morphological processing, and thinning processing.

The results from an implant test phantom image showed that we could visually confirm the detection of implant body, extraction of the skeletal features and the skeletal structure surrounding the implant with variation over five levels from coarse to dense, by thinning processing (Fig. 5). It was then verified from the measurement results of Sk.Ar/T.Ar and TSL/T.Ar that the test phantom image simulated the trabecular changes with high precision (Fig. 6). However, the results of analyzing the test phantom image showed that high correlation with the simulated changes in the trabecular bone was found only for the parameters consisting of the number of Nd (N.ImNd) integrated with the implant body and the strut lengths connecting Nd to the implant (ImNd). The parameters relating to Tm were unable to reflect the simulated changes in the trabecular bone (N.ImTm, ImTm). In addition, N.Im, which is related to both the Tm and Nd parameters, showed a strong correlation with a coefficient of 0.86. The reason for this is that the regression coefficient for N.ImNd was 0.948, indicating a nearly proportional relationship. Conventionally, in node-strut analysis, the Nd-related parameters express the continuity of the trabecular bone, while the Tm-related parameters express the discontinuity of the trabecular bone. However, Tm is defined in two dimensions, and even if Tm is present on the image we cannot rule out that in three dimensions it is connected to the trabecular bone. That is, there is a possibility that in three dimensions Tm cannot be called Tm. Therefore, it can be surmised that the Nd-related parameters reflect the three-dimensional trabecular structure better than the Tm-related parameters. The test phantom images that we employed in the present studies were simple simulations of the quantitative variation in the trabecular bone that had completed integration with the implant body. In actual clinical applications, complex bone remodeling phenomena occur in the boundary region between the implant and the trabecular bone. It will be necessary to clinically verify the degree to which the Nd-related parameters generated with our newly devised system reflect the actual processes that occur from the initial bone tissue response through the remodeling of the bone. Furthermore, when obtaining digital image information in the clinical field, there will unavoidably be sensitive distortion and displacement in standardized radiography. It will also probably be necessary to verify whether or not such distortion and displacement in geometric position influence the analytical results. In some cases, it may be necessary to add other capabilities in order to compensate for positional distortion and displacement.

The experimental results from test chart and phantom images indicate that this new diagnostic system, which combines detection of the implant body, morphological processing, a thinning process and improved node-strut analysis, could be useful

as a computer-assisted diagnosis for evaluating implant osseointegration.

References

1. Meredith N., Friberg B., Sennerby L., and Aparicio C.: Relationship between contact time measurements and PTV values when using the Periotest to measure implant stability. Int J Prosthodont 11：269–275, 1998.
2. Sunden S., Grondahl K., and Grondahl H.G.: Accuracy and precision in the radiographic diagnosis of clinical instability in Branemark dental implants. Clin Oral Implants Res 3：220–226, 1995.
3. Johansson C.B., Sennerby L., and Albrektsson T.: A removal torque and histomorphometric study of bone tissue reactions to commercially pure titanium and Vitallium implants. Int J Oral Maxillofac Implants 6：437–441, 1991.
4. Johansson P., and Strid K.G.: Assessment of bone quality from cutting resistance during implant surgery. Int J Oral Maxillofac Implants 9：279–288, 1994.
5. Friberg B., Sennerby L., Roos J., and Lekholm U.: Identification of bone quality in conjunction with insertion of titanium implants. Clin Oral Implants Res 6：213–219, 1995.
6. Kaneko T.: Theoretical percussion force of the periotest diagnosis. Int J Oral Maxillofac Implants 13：97–101, 1998.
7. Granin A.N., DeGrado J., Kaufman M., Baraoidan M., DiGregorio R., Batgitis G., and Lee Z.: Evaluation of the Periotest as a diagnostic tool for dental implants. J Oral Implantol 24：139–146, 1998.
8. Meredith N.: Assessment of implant stability as a prognostic determinant. Int J Prosthodont 11：491–501, 1998.
9. Rasmusson L., Meredith N., Kahnberg K.E., and Sennerby L.: Stability assessments and histology of titanium implants placed simultaneously with autogenous onlay bone in the rabbit tibia. Int J Oral Maxillofac Surg 27：229–235, 1998.
10. Sennerby L., and Meredith N.: Resonance frequency analysis: measuring implant stability and osseointegration. Compend Contin Educ Dent 19：493–502, 1998.
11. Friberg B., Sennerby L., Linden B., Grondahl K., and Lekholm U.: Stability measurements of one-stage Branemark implants during healing in mandibles. A clinical resonance frequency analysis study. Int J Oral Maxillofac Surg 28：266–272, 1999.
12. Friberg B., Sennerby L., Meredith N., and Lekholm U.: A comparison between cutting torque and resonance frequency measurements of maxillary implants. A 20-month clinical study. Int J Oral Maxillofac Surg 28：297–303, 1999.
13. Rasmusson L., Meredith N., Cho I.H., and Sennerby L.: The influence of simultaneous versus delayed placement on the stability of titanium implants in onlay bone grafts. A histologic and biomechanic study in the rabbit. Int J Oral Maxillofac Surg 28：224–231, 1999.
14. Rasmusson L., Stegersjo G., Kahnberg K.E., and Sennerby L.: Implant stability measurements using resonance frequency analysis in the grafted maxilla: a cross-sectional pilot study. Clin Implant Dent Relat Res 1：70–74, 1999.
15. Huang H.M., Lee S.Y., Yeh C.Y., and Lin C.T.: Resonance frequency assessment of dental implant stability with various bone qualities: a numerical approach. Clin Oral Impl Res 13：65–74, 2002.
16. Sul Y.T., Johansson C.B., Jeong Y., Wennerberg A., and Albrektsson T.: Resonance frequency and removal torque analysis of implants with turned and anodized surface oxides. Clin Oral Impl Res 13：252–259, 2002.
17. Meredith N., Alleyne D., and Cawley P.: Quantitative determination of the stability of the implant-tissue interface using resonance frequency analysis. Clin Oral Impl Res 7：261–267, 1996.
18. Meredith N., Book K., Friberg B., Jemt T., and Sennerby L.: Resonance frequency measurements of implant stability in vivo. A cross-sectional and longitudinal study of resonance frequency measurements on implants in the edentulous and partially dentate maxilla. Clin Oral Implants Res 8：226–233, 1997.
19. Adams R.D., and Cawley P.: Vibration techniques in nondestructive testing. Academic Press, London, 1985, pp.304–318.
20. Tyndall D.A., and Brooks S.L.: Selection criteria for dental implant site imaging: a position paper of the American Academy of Oral and Maxillofacial radiology. Oral Surg Oral Med Oral Pathol Oral Radiol Endod 89：630–637, 2000.
21. Harris D., Buser D., Dula K., Grondahl K., Haris D., Jacobs R., Lekholm U., Nakielny R., van Steenberghe D., and van der Stelt P.: European Association for Osseointegration. E.A.O. guidelines for the use of diagnostic imaging in implant dentistry. A consensus workshop organized by the European Association for Osseointegration in Trinity College Dublin. Clin Oral Implants Res 13：566–570, 2002.
22. Turkyilmaz I., Tozum T.F., Tumer C., and Ozbek E.N.: Assessment of correlation between computerized tomography values of the bone, and maximum torque and resonance frequency values at dental implant placement. J Oral Rehabil 33：881–888, 2006.
23. Handelsman M.: Surgical guidelines for dental implant placement. Br Dent J 201：139–152, 2006.
24. Miyamoto I., Tsuboi Y., Wada E., Suwa H., and Iizuka T.: Influence of cortical bone thickness and implant length on

implant stability at the time of surgery-clinical, prospective, biomechanical, and imaging study. Bone 37：776–780, 2005.
25. Ikumi N., and Tsutsumi S.: Assessment of correlation between computerized tomography values of the bone and cutting torque values at implant placement: a clinical study. Int J Oral Maxillofac Implants 20：253–260, 2005.
26. Herrmann I., Lekholm U., Holm S., and Kultje C.: Evaluation of patient and implant characteristics as potential prognostic factors for oral implant failures. Int J Oral Maxillofac Implants 20：220–230, 2005.
27. Homolka P., Beer A., Birkfellner W., Nowotny R., Gahleitner A., Tschabitscher M., and Bergmann H.: Bone mineral density measurement with dental quantitative CT prior to dental implant placement in cadaver mandibles: pilot study. Radiology 224：247–252, 2002.
28. Gray C.F., Redpath T.W., and Smith F.W.: Low-field magnetic resonance imaging for implant dentistry. Dentomaxillofac Radiol 27：225–229, 1998.
29. Hassfeld S., Fiebach J., Widmann S., Heiland S., and Muhling J.: Magnetic resonance tomography for planning dental implantation. Mund Kiefer Gesichtschir 5：186–192, 2001. (German)
30. Imamura H., Sato H., Matsuura T., Ishikawa M., and Zeze R.: A comparative study of computed tomography and magnetic resonance imaging for the detection of mandibular canals and cross-sectional areas in diagnosis prior to dental implant treatment. Clin Implant Dent Relat Res 6：75–81, 2004.
31. Salvolini E., De Florio L., Regnicolo L., and Salvolini U.: Magnetic Resonance applications in dental implantology: technical notes and preliminary results. Radiol Med (Torino) 103：526–529, 2002.
32. Zabalegui J., Gil J.A., and Zabalegui B.: Magnetic resonance imaging as an adjunctive diagnostic aid in patient selection for endosseous implants: preliminary study. Int J Oral Maxillofac Implants 5：283–287, 1990.
33. Kaneda T., Ogura I., Sakurai T., Kashima I., Kurita H., and Kurashina K.: Development of Mapping Sheet for Assessment of Bone Quality of the Jaw. Dentistry in Japan 40：100–105, 2004.
34. Sakoda S., Kawamata R., Kaneda T., and Kashima I.: Application of the digital radiographic bone trabecular structure analysis to the mandible using morphological filter. Oral Science International 1：45–53, 2004.
35. Watanabe A., Sakurai T., Kumasaka S., and Kashima I.: Quantitative analysis of bone trabecular structural change using X-ray bone morphometric analysis: a correlation between structural change and structural parameters. Oral Radiol 20：49–56, 2004.
36. Asa K., Kumasaka S., Sakurai T., Kashima I.: Evaluating two-dimensional skeletal structure parameters using radiological bone morphometric analysis. Oral Radiol 21：30–37, 2005.
37. Asai H., Kozai Y., Matsumoto Y., Kawamata R., Kumasaka S., Sakurai T., and Kashima I.: Radiological morphometric analysis of the mandibular bone structure after ovariectomy in mature cynomolgus monkeys. Oral Science International 2：54–63, 2005.
38. Vesterby A., Gundersen H.J., and Melsen F.: Star volume of marrow space and trabeculae of the first lumbar vertebra: sampling efficiency and biological variation. Bone 10：7–13, 1989.
39. Vesterby A.: Star volume of marrow space and trabeculae in iliac crest: sampling procedure and correlation to star volume of first lumbar vertebra. Bone 11：146–155, 1990.